J Mol Model (2014) 20:2180
DOI 10.1007/s00894-014-2180-1

ORIGINAL PAPER

Mechanical, electronic, and optical properties of Bi_2S_3 and Bi_2Se_3 compounds: first principle investigations

Husnu Koc · Hacı Ozisik · Engin Deligöz · Amirullah M. Mamedov · Ekmel Ozbay

Received: 1 August 2013 / Accepted: 11 February 2014 / Published online: 16 March 2014

Abstract The structural, mechanical, electronic, and optical properties of orthorhombic Bi_2S_3 and Bi_2Se_3 compounds have been investigated by means of first principles calculations. The calculated lattice parameters and internal coordinates are in very good agreement with the experimental findings. The elastic constants are obtained, then the secondary results such as bulk modulus, shear modulus, Young's modulus, Poisson's ratio, anisotropy factor, and Debye temperature of polycrystalline aggregates are derived, and the relevant mechanical properties are also discussed. Furthermore, the band structures and optical properties such as real and imaginary parts of dielectric functions, energy-loss function, the effective number of valance electrons, and the effective optical dielectric constant have been computed. We also calculated some nonlinearities for Bi_2S_3 and Bi_2Se_3 (tensors of elasto-optical coefficients) under pressure.

Keywords Band structure · Bi_2S_3 · Bi_2Se_3 · Elastic constants · Mechanical properties · Optical properties

H. Koc (✉)
Department of Physics, Siirt University, 56100 Siirt, Turkey
e-mail: husnu_01_12@hotmail.com

H. Ozisik
Department of Computer and Instructional Technologies Teaching, Aksaray University, 68100 Aksaray, Turkey

E. Deligöz
Department of Physics, Aksaray University, 68100 Aksaray, Turkey

A. M. Mamedov · E. Ozbay
Nanotechnology Research Center (NANOTAM), Bilkent University, 06800 Bilkent, Ankara, Turkey

Introduction

Topological insulators are materials that have a bulk band gap similar to commonly known insulators, but have conducting states on their edge or surface. The bulk band gap is generated because of the strong spin-orbit coupling inherent to these system, which also modified them in a fundamental way, leading to unconventional spin polarized Dirac fermions on the boundary of the insulator [1–3]. The single Dirac cone surface state on these compounds constitutes the simple manifestation of 2D and 3 D topological insulators. Many of the interesting theoretical proposals that utilize topological insulator surfaces require the chemical binding potential to lie at or near the surface Dirac point, and consequently bulk doping is commonly used to tune the chemical potential to the Dirac point [3, 4].

Recent theoretical and experimental progress in this area has demonstrated the existence of a novel class of bulk insulators with conducting states on their boundaries or surfaces [1–4]. Over the past few years the topological states of Bi2X3 (X=Te,Se, S), the "second generation" topological insulators, has become the focus of intense research. Motivated by their application potential (photovoltaic, thermoelectric, X-ray computed tomography, electrochemical hydrogen storage etc.)[5–9] the binary compounds Bi2X3 are the most studied. These compounds with the space group Pnma – D2h16 have four molecules (20 atoms) in a unit cell and have tetradymite-like layered structure with ionic-covalent bounded quintuple layer slabs. The earlier reported band gap of bulk Bi2S3 is 1.3 eV [10]. The most recent value of the band gap is reported to be in the range 1.3 – 1.7 eV [11], which lies in the visible solar energy spectrum [12, 13]. It has a large absorption coefficient. Bi2X3 compounds have been widely used in TV cameras with photoconducting targets, thermoelectric devices, micro- and optoelectronic devices, and IR spectroscopy [14–22]. Also, Bi2X3 compounds have been shown to be ideal candidates for studying room temperature topological

insulating behavior as they have the topologically non-trivial band gap [3], much larger than the room temperature energy scale [3]. Therefore, Bi2X3 compounds are considered to be a promising topological system toward unique applications in next generation electronics [3].

In the past, the structural and electronic properties of these compounds were analyzed in detail by different authors [23–28]. The valance electron density, electron band structure, and corresponding electronic density-of-states (DOS) of X_2Y_3 (X = Bi, Sb and Y = S, Se) compounds using the density functional theory were studied by Caracas et al. [23]. Sharma et al. [24] computed the energy band, density of states and optical properties of orthorhombic Bi_2S_3 and rhombohedral Bi_2Se_3 using the gradient approximation (GGA) in the frame density functional theory. Sharma et al. [25] investigated the structural, electronic and optical properties of the trigonal and orthorhombic phases of Bi_2Se_3 using the density functional theory based on full-potential linearized augmented plane wave (LAPW) + local orbitals (lo). Olsen et al. [26] provided an analysis of the electronic structure using SIESTA DFT code calculations for $Cu_4Bi_5S_{10}$ and Bi_2S_3. Filip et al. [27] investigated the quasiparticle structural properties, band structures, and band gaps using the first principles GW and LDA approximations. Zhao et al. [28] predicted a series of Raman-active photon modes using a first principle calculation for the vibrational modes of Bi_2S_3.

To our knowledge, the mechanical properties, optical properties except for the real and imaginary parts of dielectric functions, and elasto-optical coefficients under pressure have not been reported in detail for Bi_2S_3 and Bi_2Se_3 so far. In this context, the mechanical properties and optical properties such as the effective number of valance electrons and the effective optical dielectric constant, and elasto-optical coefficients under pressure of these compounds are the first required data for any eventual applications of the material in topological insulators. Also, the features of the spectrum with degeneracy of the symmetric points of the Brillouin zone were discussed for crystalline three-dimensional → two dimensional, two-dimensional → one-dimensional, and pure two-dimensional systems [29]. Conical features of the spectrum were detected in three–dimensional → two-dimensional systems (hetere bound arises between V-VI semiconductors with band inversion) [30]. A question arises of whether conical features exist in crystalline systems like topological insulators with a higher degree of degeneracy. Therefore, in the present paper we also discussed the states with the conic dispersion law and with more than twofold degeneracy in Bi2X3.

Methods

Simulations of Bi_2S_3 and Bi_2Se_3 compounds were conducted, using two different quantum mechanical (QM) DFT programs. The first, freely accessible code, SIESTA combines norm conserving pseudopotentials with the local basis functions. First principles calculations within the general framework of the density functional theory of the system on the molecular basis set based on the finite range pseudoatomic orbitals (PAOs) of the Sankey_Niklewsky type [31], generalized to include multiple-zeta decays were performed. The calculations of the total energies and atomic forces are done in a linear combination of atomic orbitals according to the standard procedures of SIESTA [32, 33]. In the calculation, the local density approximation (LDA) [34] for the exchange-correlation [35, 36] energy was used. The basis set used in the present study was double-zeta plus polarization. Siesta calculates the self-consistent potential on a grid in real space. The fineness of this grid is determined in terms of an energy cut-off E_c in analogy to the energy cut-off when the basis set involves plane waves. We found an optimal value of around 375 *Ry* between 100 and 450 *Ry* cut-off energies with various basis sets for Bi_2S_3 and Bi_2Se_3; 256 k-points for Bi_2S_3 and Bi_2Se_3 were enough to obtain the converged total energies.

The interactions between electrons and core ions are simulated with separable Troullier-Martins [37] norm-conserving pseudopotentials. We have generated atomic pseudopotentials separately for atoms Bi, S, and Se by using the $6s^26p^3$, $3s^23p^4$, and $4s^24p^4$ configurations, respectively. For present atomic pseudopotentials, the cut-off radii are taken as s: 1.60 au, p: 1.73 au, 1.90 au for the d and f channels of S, s: 1.91 au, p: 2.10 au, d: 1.91 au f: 2.44 of Se and s: 3.82 au, p: 2.71 au, 2.92 au for the d and f channels of Bi.

The second, commercially available (VASP) [38–41], code employs plane wave basis functions. The calculations performed with this code and reported here also use the LDA. The electron-ion interaction was considered in the form of the projector-augmented-wave (PAW) method with a plane wave up to an energy of 450 eV [41, 42]. This cut-off was found to be adequate for studying the structural and elastic properties. The 8x11x8 Monkhorst and Pack [43]grid of k-points have been used for these compounds.

Results and discussion

Structural properties

The structures of Bi_2S_3 and Bi_2Se_3 are considered as an orthorhombic structure. These crystals have four Bi_2X_3 (X = S, Se) molecules (20 atoms) in unit cell. The positions corresponding to the orthorhombic Bi_2S_3 and Bi_2Se_3 have been obtained from experimental data [23, 44, 45]. The calculated atomic positions are given in Table 1. For SIESTA calculations, the equilibrium lattice parameters, bulk modulus, and its pressure derivative were obtained by minimizing the total energy for the different values of the lattice parameters by

means of Murnaghan's equation of states (EOS) [46]. For the VASP calculations, the cell volume and ionic positions of atoms in reciprocal coordinates for the considered compounds were fully relaxed. The results for the SIESTA and VASP calculations are shown in Table 2 along with the experimental and theoretical values. The obtained lattice parameters using both the code for Bi_2S_3 and Bi_2Se_3 are in good agreement with the experimental and theoretical values. We confirmed that the calculated results are similar between the VASP and SIESTA calculations. In the SIESTA code, the calculated bulk moduli for Bi_2S_3 and Bi_2Se_3 are 78.82 and 70.70 GPa, respectively.

Elastic properties

The elastic constant C_{ij} of solids provides a link between the mechanical and dynamical behavior of crystals, and some of the more important information that can be obtained from ground state total energy calculations. The C_{ij} determine the response of the crystal to external forces characterized by the bulk modulus, Young's modulus, shear modulus, and Poisson's ratio and, therefore, play an important part in determining the stability and stiffness of the materials [47, 48].

The present elastic constants are computed by using the "volume-conserving" technique [49] and the strain–stress relationship [50] for SIESTA and VASP calculations, respectively. The obtained C_{ij} for SIESTA and VASP calculations are summarized in Table 3. The elastic constant values of SIESTA are, generally, in accordance with the elastic constant values of VASP. Unfortunately, there are no theoretical results for comparing them with the present work. However, our results can serve as a prediction for future investigations.

The mechanical stability criteria for orthorhombic structures are given in ref. [51]. The present elastic constants in Table 3 obey these stability conditions for orthorhombic Bi_2S_3 and Bi_2Se_3. The elastic constants C_{11}, C_{22}, and C_{33} measure the *a*-, *b*-, and *c*-direction resistance to linear compression, respectively. The C_{11} for SIESTA calculations is lower than the C_{22} and C_{33} while the C_{33} for VASP calculations of Bi_2S_3 is lower than the C_{11} and C_{22}. The calculated C_{33} of both codes for Bi_2Se_3 are lower than the C_{11} and C_{22}. Thus, Bi_2S_3 compound is more compressible along the *a*-axis and *c*-axis for SIESTA and VASP calculations, respectively, while the Bi_2Se_3 compound is more compressible along the *c*-axis for SIESTA and VASP calculations.

It is known that, the elastic constant C_{44} is the most important parameter indirectly governing the indentation hardness of a material. The large C_{44} means a strong ability to resist the monoclinic shear distortion in (100) plane, and the elastic constant C_{66} relates to the resistance to shear in the <110> direction. In the present case, C_{44}, C_{55}, and C_{66} for both codes of Bi_2Se_3 are lower than the Bi_2S_3 compound.

There are two approximation methods to calculate the polycrystalline modulus, namely, the Voigt method [52] and the Reuss method [53]. Using the common relations [54, 55], the Hill average [56] was used to calculate the polycrystalline modulus in a manner similar to our recent works [57, 58]. Table 4 shows the calculated bulk modulus, shear modulus, Young's modulus, and Poisson's ratio. The bulk modulus is a measure of resistance to volume change by an applied pressure, whereas the shear modulus is a measure of resistance to reversible deformations upon shear stress [59]. Hence, shear modulus exhibits better correlations with hardness than the bulk modulus. The calculated shear modulus and bulk modulus for SIESTA (VASP) are 43.2 (45.2), 67.8 (83.6) GPa and 39.4 (39.0), 65.7 (71.9) GPa for Bi_2S_3 and Bi_2Se_3, respectively. The values of the bulk moduli indicate that Bi_2S_3 is a less compressible material than the Bi_2Se_3 compound. The calculated shear modulus for Bi_2Se_3 is lower than Bi_2S_3 compound. The calculated bulk moduli using elastic constants are lower (about 7.51 % and 3.67 %, respectively) than the other bulk moduli (67.8 and 65.7 for Bi_2S_3 and Bi_2Se_3, respectively) using EOS.

The criterion in refs. [59, 60] for ductility or brittleness is the value of the *B*/*G*. If the *B*/*G* ratio is higher (less) than, 1.75, then a material is ductile (brittle). The *B*/*G* ratio calculated for SIESTA is lower than 1.75 while the *B*/*G* ratio calculated for VASP is higher than 1.75 for both compounds. Hence, both compounds behave in a brittle (ductile) manner for SIESTA (VASP). Therefore, further study is necessary to solve the discrepancy.

Young's modulus, which is defined as the ratio of stress and strain is used to provide for the measurement of the stiffness of the solid. The higher the value of Young's modulus, the stiffer the materials is. Here, the value of Young's modulus (106.9 GPa for SIESTA and 114.8 GPa for VASP) of the Bi_2S_3 compound is higher than Bi_2Se_3 (98.5 GPa for SIESTA and 99.0 GPa for VASP). Therefore, the Bi_2S_3 compound is relatively stiffer than Bi_2Se_3. If the value of *E*, which has an impact on the ductile, increases, then covalent nature of the material also increases. In Table 4, it is shown that *E* increases as you move from Bi_2Se_3 to Bi_2S_3.

The value of Poisson's ratio is indicative of the degree of directionality of the covalent bonds. The value of the Poisson's ratio is small (υ =0.1) for covalent materials, whereas for ionic materials a typical value of υ is 0.25 [61]. The calculated Poisson's ratios of SIESTA and VASP are approx. 0.24, 0.27 and 0.25, 0.27 for Bi_2S_3 and Bi_2Se_3, respectively. Therefore, the ionic contribution to inter atomic bonding for these compounds is dominant. The υ=0.25 and 0.5 are the lower and upper limits, respectively, for central force solids [62]. For Bi_2S_3 and Bi_2Se_3, the values of υ are close to 0.25, indicating that interatomic forces are weightless central forces.

In the crystal structures, elastic anisotropy is important in understanding the elastic properties [63]. The shear anisotropic factors on different crystallographic planes provide a measure of the degree of anisotropy in atomic bonding in different

Table 1 The calculated internal coordinates together with experimental value

Space group: Pnma—orthorhombic		Experimental [23, 44, 45]			Present-SIESTA			Present-VASP		
Atomic positions										
Atom	Wyckoff	x	y	z	x	y	z	x	y	z
Bi_1	4c	0.517	0.25	0.175	0.503	0.24	0.175	0.502	0.25	0.176
Bi_2	4c	0.660	0.75	0.466	0.660	0.76	0.459	0.672	0.75	0.472
S_1	4c	0.623	0.75	0.058	0.619	0.76	0.059	0.623	0.75	0.056
S_2	4c	0.715	0.25	0.306	0.712	0.24	0.299	0.721	0.25	0.301
S_3	4c	0.451	0.75	0.373	0.446	0.76	0.363	0.447	0.75	0.369
Bi_1	4c	0.512	0.25	0.172	0.502	0.25	0.173	0.502	0.25	0.172
Bi_2	4c	0.657	0.75	0.466	0.664	0.75	0.469	0.664	0.75	0.464
Se_1	4c	0.630	0.75	0.056	0.627	0.75	0.055	0.627	0.75	0.056
Se_2	4c	0.713	0.25	0.307	0.721	0.25	0.299	0.721	0.25	0.299
Se_3	4c	0.433	0.75	0.376	0.444	0.75	0.367	0.445	0.75	0.367

planes. The shear anisotropic factors for the {100}, {010}, and {001} shear planes are given by $A_1=4C_{44}/(C_{11}+C_{33}-2C_{13})$, $A_2=4C_{55}/(C_{22}+C_{33}-2C_{23})$, and $A_3=4C_{66}/(C_{11}+C_{22}-2C_{12})$. The calculated A_1, A_2 and A_3 of both codes for Bi_2S_3 and Bi_2Se_3 are given in Table 5. A value of unity means that the crystal exhibits isotropic properties while values other than unity represent varying degrees of anisotropy. From Table 5, it can be seen that Bi_2S_3 and Bi_2Se_3 exhibit larger anisotropy in the {100} and {010} shear planes. For polycrystalline, we also calculate the percentage of anisotropy defined as [61, 62, 64] $A_B=(B_V-B_R)/(B_V+B_R)$ and $A_G=(G_V-G_R)/(G_V+G_R)$ in the compression and shear, respectively.

For an isotropic crystal, these values can range from zero (isotropic) to 100 % representing the maximum anisotropy. A_B and A_G values for Bi_2S_3 and Bi_2Se_3 have been computed, and results are listed in Table 5. It can also be seen that the anisotropy in compression is small and the anisotropy in shear is high. Bi_2S_3 compound in SIESTA code exhibits relatively high shear and bulk anisotropies compared with the Bi_2Se_3 compound. The results obtained with VASP code are the exact opposite of the results obtained from SIESTA code. Hence, further study is necessary to solve the discrepancy.

One of the standard methods for calculating the Debye temperature is to use elastic constant data since θ_D [65] may be estimated from the average sound velocity (v_m). At low temperatures, we have calculated the sound velocities and the Debye temperature by using the common relation given in refs. [66, 67] for Bi_2S_3 and Bi_2Se_3, and the results are listed in Table 6 along with the calculated values of density.

For materials, it is usually the case that the higher the Debye temperature is the higher microhardness will be. As can be seen in Table 6, the Debye temperature for Bi_2S_3 is

Table 2 The calculated equilibrium lattice parameters (a, b, and c), bulk modulus (B), and the pressure derivative of bulk modulus (B') together with the theoretical and experimental values for Bi_2S_3 and Bi_2Se_3

Material	Reference	a (Å)	b (Å)	c (Å)	B (GPa)	B'
Bi_2S_3	Present (SIESTA)	11.314	3.980	11.014	78.82	4.37
	Present (VASP)	10.999	3.940	10.825		
	Theory (QUANTUM ESPRESSO) [a]	11.227	3.999	11.001		
	Theory (QUANTUM ESPRESSO)[b]	10.950	3.974	11.103		
	Experimental[c]	11.305	3.981	11.147		
Bi_2Se_3	Present (SIESTA)	11.763	4.106	11.476	70.70	4.75
	Present (VASP)	11.505	4.079	11.302		
	Theory (QUANTUM ESPRESSO) [a]	11.767	4.141	11.491		
	Experimental[d]	11.830	4.090	11.620		

[a] Ref [27]

[b] Ref [28]

[c] Ref [44]

[d] Ref [45]

Table 3 The calculated elastic constants (in GPa) for Bi_2S_3 and Bi_2Se_3

Material	Reference	C_{11}	C_{22}	C_{33}	C_{12}	C_{13}	C_{23}	C_{44}	C_{55}	C_{66}
Bi_2S_3	Present (SIESTA)	93.8	135.5	108.7	33.3	50.9	56.5	69.8	57.7	37.8
	Present (VASP)	132.7	140.2	123.3	47.1	62.4	69.3	69.3	55.8	39.4
Bi_2Se_3	Present (SIESTA)	110.9	107.6	96.1	38.4	48.1	51.8	62.4	51.2	35.9
	Present (VASP)	116.7	115.4	107.8	39.2	54.6	60.4	60.9	49.0	33.9

higher than that for Bi_2Se_3. The Debye temperatures obtained with VASP code are compatible with that obtained from SIESTA code.

Electronic properties

The investigation of the electronic band structure for understanding the electronic and optical properties of Bi_2S_3 and Bi_2Se_3 is very useful. The band structures of the orthorhombic Bi_2S_3 and Bi_2Se_3 in the SIESTA code are calculated using LDA approximation. The electronic band structures were calculated along the special lines connecting the high-symmetry points S (½,½,0), Y (0,½,0), Γ (0,0,0), X (½,0,0), S(½,½,0), R (½,½,½) for Bi_2S_3 and Bi_2Se_3 in the k-space. The energy band structures calculated for Bi_2S_3 and Bi_2Se_3 are shown in Fig. 1. As can be seen in Fig. 1a, the Bi_2S_3 compound has an indirect band gap semiconductor with the value 1.32 *eV* (see Table 7). The top of the valance band is positioned near the X point between Γ and X point of BZ, and the bottom of the conduction band is located at the Γ point of BZ. The band gap value obtained for Bi_2S_3 is less than some of the estimated experimental and theoretical results and the band gap has the same character as given in ref. [68, 69]. The present band and the density of states (DOS) profiles for Bi_2S_3 agree with the earlier work [24].

It can be seen from Fig. 1b that the band gap of Bi_2Se_3 compound has the same character as that of Bi_2S_3. The top of the valance band and the bottom of the conduction band are located near the Γ point between Y and Γ point of BZ, and near the X point between the Γ and X point of BZ, respectively. The indirect band gap value of Bi_2Se_3 compound is 0.95 *eV* (see Table 7). The band gap value obtained for Bi_2Se_3 is bigger than the estimated theoretical results. Unfortunately, there are no experimental results to compare with the calculated band gap value.

The total and partial densities of states corresponding to the band structures of Bi_2S_3 and Bi_2Se_3 are calculated and the results are indicated in Figs. 2 and 3 along with the Fermi energy level, respectively. In these figures, the lowest valence bands that occur between approximately -15 and -12 *eV* are dominated by S 3s and Se 4s states while the valence bands that occur between approximately -12 and -8 *eV* are dominated by Bi 6s states. The highest occupied valance bands are essentially dominated by S 3p and Se 4p states. The 6p states of Bi atoms also contribute to the valance bands, but the values of the densities of these states are rather small compared to S 3p and Se 4p states. The lowest unoccupied conduction bands just above Fermi energy level is dominated by Bi 6p. The 3p (4p) states of S (Se) atoms also contribute to the conduction bands, but the values of densities of these states are rather small compared to Bi 6p states.

The band structures of Bi_2S_3 and Bi_2Se_3 crystals were compared because the band structures of these crystals highly resemble one another. Thus, on the formation of the band structures (it seems to us) of Bi_2S_3 and Bi_2Se_3 the 6s 6p orbitals of Bi atoms are more dominant than the 3s3p and 4s4p orbitals of S and Se atoms.

It is well known that interband contributions to ε can be accurately fitted to a single-oscillator Sellmeier expression for which reliable refractive-index dispersion data are available. For an arbitrary light-polarization direction, the wavelength dependence of ε is given closely by the relation: [73]

$$\varepsilon - 1 = S_0(\lambda_0)^2 / \left[1 - (\lambda_0/\lambda)^2\right] \quad (1)$$

Table 4 The calculated isotropic bulk modulus (B, in GPa), shear modulus (G, in GPa), Young's modulus (E, in GPa), and Poisson's ratio for Bi_2S_3 and Bi_2Se_3 compounds

Material	Reference	*B*	*G*	*E*	υ	*G*/*B*	*B*/*G*
Bi_2S_3	Present (SIESTA)	67.8	43.2	106.9	0.2372	0.637	1.569
	Present (VASP)	83.6	45.2	114.8	0.2709	0.540	1.849
Bi_2Se_3	Present (SIESTA)	65.7	39.4	98.5	0.2501	0.599	1.668
	Present (VASP)	71.9	39.0	99.0	0.2703	0.542	1.843

Table 5 The calculated shear anisotropic factors A_1, A_2, A_3, and A_B, A_G

Material	Reference	A_1	A_2	A_3	A_B (%)	A_G (%)
Bi_2S_3	Present (SIESTA)	2.77	1.76	0.93	1.52	6.38
	Present (VASP)	2.11	1.79	0.88	0.10	4.82
Bi_2Se_3	Present (SIESTA)	2.25	2.05	1.02	0.01	5.79
	Present (VASP)	2.11	1.92	0.88	0.12	5.36

Here, λ is the light wavelength and S_0 and λ_0 are oscillator strength and position parameters, respectively. The interband energy ($\varepsilon_0=hc/e\lambda_0$) and interband strength [$F=(hc/e)^2S_0$] parameters are physically meaningful (h is Planck's constant, c is the speed of light, and e is the electronic charge). Using these parameters we can define a "dispersion energy" ε_d given by $\varepsilon_d=F/\varepsilon_0=(hc/e)S_0\lambda_0$ and all the other Sellmeier parameters for Bi_2S_3 and Bi_2Se_3 ("dispersion energy" determines the dispersion of the electronic dielectric constant in nonmetallic nonmagnetic solids). The dispersion energies of Bi_2S_3 and Bi_2Se_3 compounds along the x, y, and z axes are 14.65 *eV*, 18.82 *eV*, 18.18 *eV* and 22.09 *eV*, 26.37 *eV*, 27.32 *eV*, respectively.

We also calculated the influence of external pressure on the electronic band structure and the band gap of Bi_2S_3 and Bi_2Se_3 (Fig. 4). It is well known that the influence of pressure on E_g for most materials in a wide pressure range is linear (Eg=Eg(0)+AP+….). Our calculations show that A= $0.64x10^{-2}eV/GPa$ (Bi_2S_3) and $1.58x10^{-2}eV/GPa$ (Bi_2Se_3) for direct optical transition in the Γ-high symmetry point. For all other high symmetry points we observed results that were very close to it.

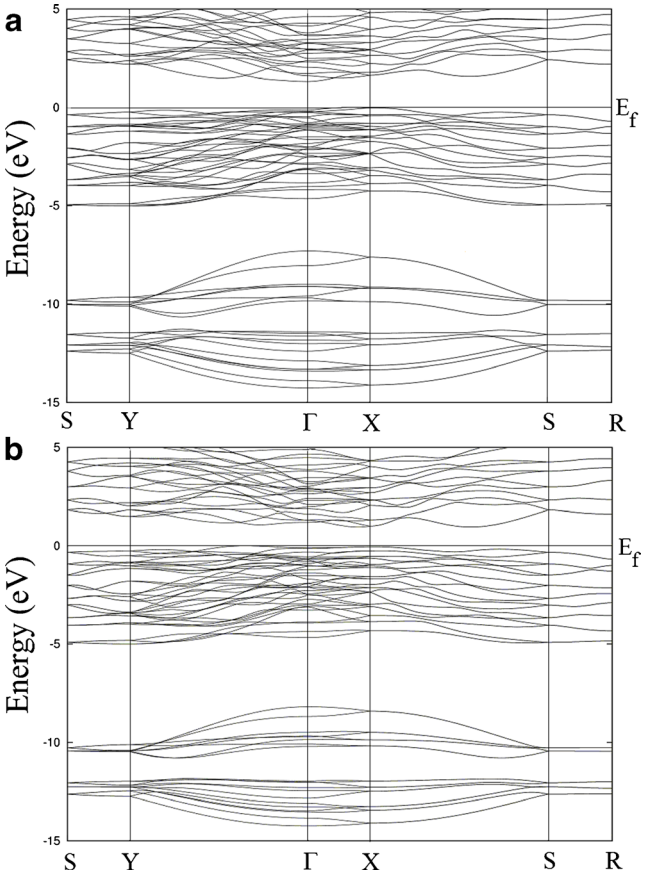

Fig. 1 Energy band structure for a) Bi_2S_3 and b) Bi_2Se_3

Optical properties

The significant point in linear and non-linear optics is that when the electromagnetic field becomes strong enough, the dielectric function becomes on the electric field vector, **E** (ω) or polarization per unit volume **P** (ω). We can calculate this polarization as [74]:

$$P^i(\omega) = \chi^{(1)}_{ij}..E^j(\omega) + \chi^{(2)}_{ijk}.E^j(\omega).E^k(\omega) + \ldots \quad (2)$$

where $\chi^{(1)}$ is the linear optical susceptibility tensor, and $\chi^{(2)}$ is the lowest order nonlinearity second susceptibility that is important in non-linear materials with no center of inversion. The other high order nonlinear susceptibilities come into play for non-linear effects in cubic crystals with a center of inversion for which the first order terms vanishes by symmetry. For the present calculations and discussion we will only consider the linear and lowest order nonlinear terms.

Now in order to find the linear and nonlinear susceptibility polarization operator P (Eq. 2) can be written as

$$\langle P\rangle = \langle P\rangle_I + \langle P\rangle_{II} + \ldots \quad (3)$$

Table 6 The density, longitudinal, transverse, and average elastic wave velocities together with the Debye temperature for Bi_2S_3 and Bi_2Se_3

Material	Reference	ρ (g/cm^3)	v_l (m/s)	v_t (m/s)	v_m (m/s)	$\theta_D(K)$
Bi_2S_3	Present (SIESTA)	6.88	4267	2504	2775	283.3
	Present (VASP)	7.28	4446	2492	2774	288.4
Bi_2Se_3	Present (SIESTA)	7.84	3882	2241	2488	244.8
	Present (VASP)	8.19	3888	2181	2427	242.3

Table 7 The calculated energy band gap with SIESTA

Material	Reference	E_g (eV)
Bi_2S_3	Present	1.32 indirect
	Experimental[a]	1.28 indirect
	Experimental[b]	1.43 indirect
	Experimental[c]	1.30 direct
	Experimental[d]	1.58 direct
	Experimental[e]	1.67 direct
	Theory[f] (DFT-GGA and FP-LAPW)	1.45 and 1.32
	Theory[g] (DFT-LDA and GW)	1.12 and 1.42 direct
	Theory[h] (DFT-LDA)	1.47
	Theory[i] (FP-LAPW)	1.24
Bi_2Se_3	Present	0.95 indirect
	Theory[h] (DFT-LDA)	0.90
	Theory[g] (DFT-LDA and GW)	0.83 and 0.91 direct

[a] Ref [68]
[b] Ref [69]
[c] Ref [70]
[d] Ref [71]
[e] Ref [72]
[f] Ref [24]
[g] Ref [27]
[h] Ref [23]
[i] Ref [22]

where

$$\langle P^i \rangle_I = \chi^{(1)}_{ij}(-\omega_\beta, \omega_\beta) e^{-i\omega\beta t} E^j(\omega_\beta) \tag{4}$$

$$\langle P^i \rangle_{II} = \chi^{(2)}_{ijk}(-\omega_\beta, -\omega_\gamma, \omega_\beta, \omega_\gamma) e^{-i(\omega_\beta+\omega_\gamma)t} E^j(\omega_\beta) E^k(\omega_\gamma) \tag{5}$$

and we get the expression for the linear susceptibility [70]

$$\chi^{(1)}_{ij}(-\omega, \omega) = \frac{e^2}{\hbar\Omega} \sum_{nm\vec{k}} f_{nm}\left(\vec{k}\right) \frac{r^i_{nm}\left(\vec{k}\right) r^i_{mn}\left(\vec{k}\right)}{\omega_{mn}\left(\vec{k}\right) - \omega} = \frac{\varepsilon_{ij}(\omega) - \delta_{ij}}{4\pi} \tag{6}$$

where n,m denote energy bands, $f_{mn}\left(\vec{k}\right) \equiv f_m\left(\vec{k}\right) - f_n\left(\vec{k}\right)$ is the Fermi occupation factor, Ω is the normalization volume. $\omega_{mn}\left(\vec{k}\right) \equiv \omega_m\left(\vec{k}\right) - \omega\left(\vec{k}\right)$ are the frequency differences, $\hbar\omega_n\left(\vec{k}\right)$ is the energy of band n at wave vector **k**.

The $\vec{r}_{nm}$ are the matrix elements of the position operator given as follows [75].

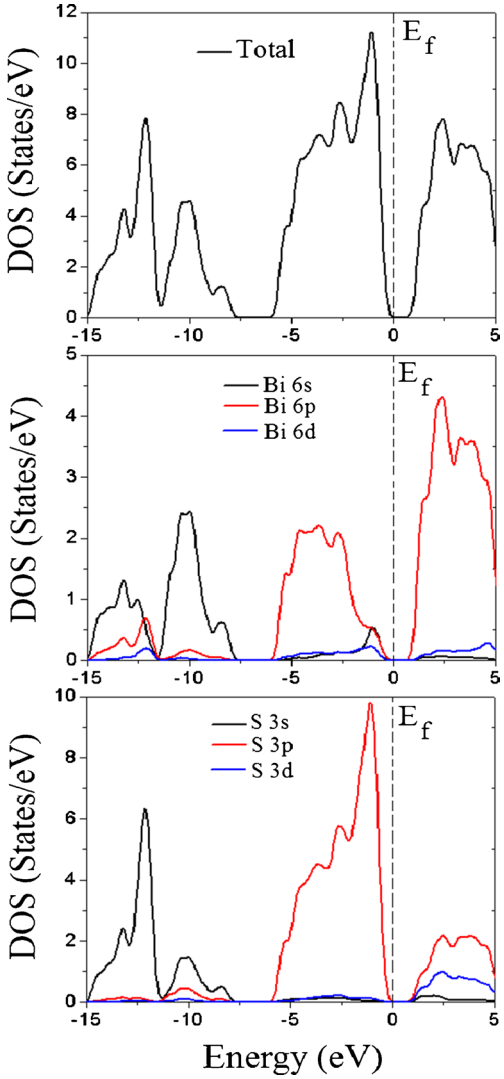

Fig. 2 The total and projected density of states for Bi_2S_3

$$\begin{aligned} \rightarrow r_{nm} &= \frac{V_{nm}\left(\rightarrow k\right)}{i\omega_{nm}\left(\rightarrow k + \rightarrow K\right)}; \omega_n \neq \omega_m \\ \rightarrow r_{nm} &= 0 \qquad ; \omega_n = \omega_m \end{aligned} \tag{7}$$

where $V_{nm}\left(\vec{k}\right) = m^{-1} p_{nm}\left(\vec{k}\right)$, m is the free electron mass, and $p_{nm}\left(\vec{k}\right)$ is the momentum matrix element. Similarly, we get the expression for the second order susceptibility [75]:

$$\begin{aligned} \chi^{(2)}_{ijk}(-\omega_\beta, -\omega_\gamma; \omega_\beta, \omega_\gamma) &= \chi^{(II)}_{ijk}(-\omega_\beta, -\omega_\gamma; \omega_\beta, \omega_\gamma) \\ &+ \eta^{(II)}_{ijk}(-\omega_\beta, -\omega_\gamma; \omega_\beta, \omega_\gamma) + \frac{i\sigma^{(II)}_{ijk}(-\omega_\beta, -\omega_\gamma; \omega_\beta, \omega_\gamma)}{(\omega_\beta + \omega_\gamma)} \end{aligned} \tag{8}$$

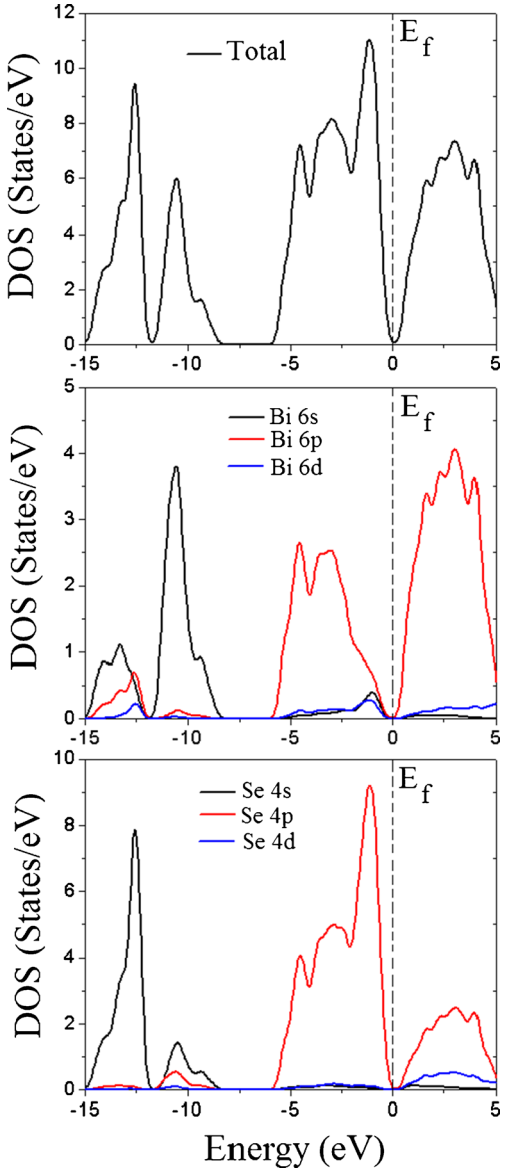

Fig. 3 The total and projected density of states for Bi_2Se_3

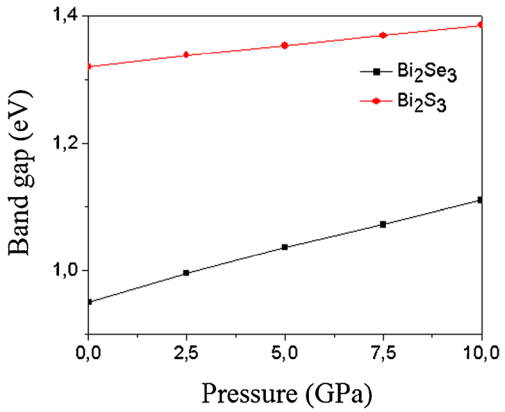

Fig. 4 The pressure variations of energy band gaps (E_g) in the Γ-high symmetry point for Bi_2S_3 and Bi_2Se_3

that includes contributions of interband and intraband transitions to the second order susceptibility.

As can be seen from Eq. (6), the dielectric function $\varepsilon_{ij}(\omega) = 1+4\pi\chi_{ij}^{(1)}(-\omega,\omega)$ and the imaginary part of $\varepsilon_{ij}(\omega), \varepsilon_2^{ij}(\omega)$, is given by

$$\varepsilon_2^{ij}(w)2 = \frac{e^2}{\hbar\,\pi}\sum_{nm}\int d\vec{k}\, f_{nm}\left(\vec{k}\right)\frac{v_{nm}^{i}\left(\vec{k}\right)v_{nm}^{j}\left(\vec{k}\right)}{\omega_{mn}^{2}}\delta\left(\omega-\omega_{mn}\left(\vec{k}\right)\right). \quad (9)$$

The real part of the dielectric function $\varepsilon_{ij}(\omega), \varepsilon_1^{ij}(\omega)$, can be calculated from Eq. (9) by using the Kramers-Kroning relations [75]. Because the Kohn-Sham equations determine the ground state properties, the unoccupied conduction bands as calculated have no physical significance. If they are used as single-particle states in the calculation of optical properties for semiconductors, a band gap problem comes into play in calculations of response. In order to take into account self-energy effects, in the present work, we used the 'scissors approximation' [74, 76].

The sum rules [77] for the finite interval of integration in terms of N_{eff} (an effective number of the valence electrons contributing to the optical properties in the same energy range):

$$N_{eff}(E) = \frac{2m\varepsilon_0}{\pi\hbar^2 e^2 Na}\int_0^{E_0}\varepsilon_2(E)EdE, \quad (10)$$

where N_a is the density of atoms in a crystal, e and m are the charge and mass of the electron, respectively.

Similarly, the effective dielectric function ε_{eff}, produced by an interband and low-lying transition (core and semi-core bands) in the same range may be written by using the same rules as

$$\varepsilon_{eff}(E)-1 = \frac{2}{\pi}\int_0^{E_0}\varepsilon_2(E)E^{-1}dE. \quad (11)$$

The physical meaning of ε_{eff} may be understood from the fact that ε_2 describes the real optical transitions plots of the effective optical dielectric constant ε_{eff} versus energy and, therefore, it is possible to estimate which transitions make the most important contribution to the static dielectric constant in the energy range from zero to E_0, i.e., by the polarization of the electron shells.

In order to calculate the optical response by using the calculated band structure, we have chosen a photon-energy range of 0-25eV and have seen that a 0-17eV photon-energy range is sufficient for most optical functions.

The Bi_2S_3 and Bi_2Se_3 single crystals have an orthorhombic structure that is optically a biaxial system. For this reason, the linear dielectric tensor of the Bi_2S_3 and Bi_2Se_3 compounds has three independent components

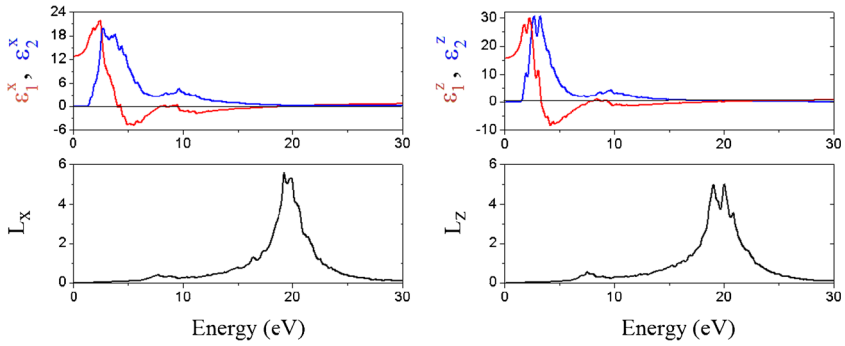

Fig. 5 Energy spectra of dielectric function $\varepsilon=\varepsilon_1-i\varepsilon_2$ and energy-loss function (L) along the x- and z-axes for Bi_2S_3

that are the diagonal elements of the linear dielectric tensor.

We first calculated the real and imaginary parts of the linear dielectric function of the Bi_2X_3 compounds along the x- and z-directions (Figs. 5 and 6). All the Bi_2X_3 compounds studied so far have $\varepsilon_1^x(\varepsilon_1^z)$ equal to zero in the energy region between $4eV$ and $20eV$ for decreasing ($d\varepsilon_1/dE<0$) and increasing ($d\varepsilon_1/dE>0$) of $\varepsilon_1(eV)$ (see, Table 8). Also, values of ε_1 versus photon energy have main peaks in the energy region between $0.5eV$ and $9eV$. Some of the principal features and singularities of the ε_{ij} for both investigated compounds are shown in Table 8. As we can see from Figs. 5 and 6, ε_1^x behaves mainly as a classical oscillator. In addition, by analogy with Bi_2X_3, one can associate the peaks of the ε_2^x and ε_2^z with the transitions between the state Γ_{15}, which is thought to be the highest valence band state at the endpoint of the Γ-directions in the Brillouin zone, and the state Γ_{21}, the lowest conduction band state for the same wave vector. The imaginary part of the dielectric function has strong peaks for Bi_2S_3 and Bi_2Se_3 in the energy region between $2eV$ and $4eV$ (see Table 8). The optical properties of Bi2X3 vary somewhat from compound to compound and from direction to direction, but show similar features for both materials because the electronic configurations of Se ([Ar],$3d^{10}$ 4 s^2 $4p^2$) and S([Ne], 3 s^2 $3p^3$) are very close to each other. In general, there are various contributions to the dielectric function, but Figs. 5 and 6 show only the contribution of the electronic polarizability to the dielectric function. The maximum peak values of ε_2^x and ε_2^z are in agreement with maximum peak values of the theoretical results for Bi_2S_3 [26]. In the range between 2 eV and 5 eV, ε_1^z decrease with increasing photon-energy, which is characteristic of an anomalous dispersion. In this energy range, the transitions between occupied and unoccupied states mainly occur between S 3p and Se 4p states which can be seen in the DOS displayed in Figs. 2 and 3. Furthermore, as can be seen from Figs. 5 and 6, the photon–energy range up to $1.5eV$ is characterized by high transparency, no absorption, and a small reflectivity. The 1.8-$5.0eV$ photon energy range is characterized by strong absorption and appreciable reflectivity. The absorption band extending beyond $10eV$ up to $15eV$ is associated with the transitions from the low-lying valance subband to the conduction band. Second, we see that above $10eV$, corresponding to the S 3s (Se 4s) and Bi 6p. In addition, we remark that the region above $15eV$ cannot be interpreted in terms of classical oscillators. Above $15eV$ ε_1 and ε_2 are dominated by linear features, increasing for ε_1 and decreasing for ε_2.

The corresponding energy-loss functions, $L(\omega)$, are also presented in Figs. 5 and 6. In this figure, L_x and L_z correspond to the energy-loss functions along the x- and z-directions. The function $L(\omega)$ describes the energy loss of fast electrons traversing the material. The sharp

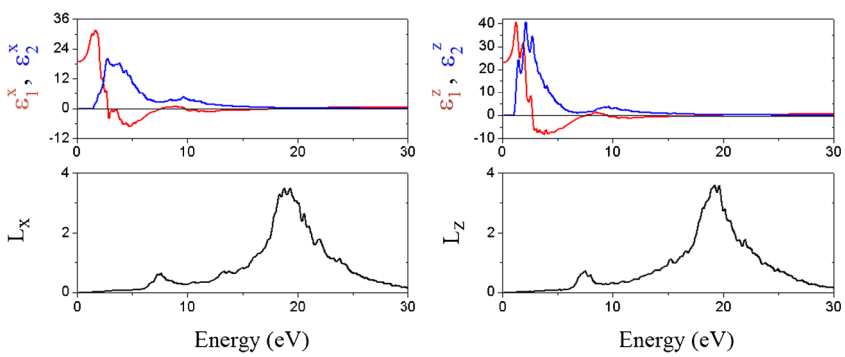

Fig. 6 Energy spectra of dielectric function $\varepsilon=\varepsilon_1-i\varepsilon_2$ and energy-loss function (L) along the x- and z-axes for Bi_2Se_3

Table 8 Some of the principal features and singularities of the linear optical responses for Bi_2S_3 and Bi_2Se_3

Material	$\varepsilon_1(eV)$	$d\varepsilon_1/dE<0$			$d\varepsilon_1/dE>0$			$\varepsilon_2(eV)$	
Bi_2S_3	ε_1^x	4.05	4.35	8.93	4.20	8.09	19.36	$\varepsilon_{2,\max}^x$	2.72
	ε_1^z	3.31	–	9.40	7.61	–	19.08	$\varepsilon_{2,\max}^z$	2.65
Bi_2Se_3	ε_1^x	2.78	–	9.71	7.63	–	18.68	$\varepsilon_{2,\max}^x$	2.05
	ε_1^z	2.70	–	9.51	7.51	–	18.84	$\varepsilon_{2,\max}^z$	2.08

maxima in the energy-loss function are associated with the existence of plasma oscillations [78]. The curves of L_x and L_z in Figs. 5 and 6 have a maximum near 19.29 and 19.04 *eV* for Bi_2S_3, respectively, and 18.74 and 19.18 *eV* for Bi_2Se_3, respectively.

The calculated effective number of valence electrons N_{eff} and the effective dielectric constant ε_{eff} are given in Fig. 7. The effective optical dielectric constant, ε_{eff}, shown in Fig. 7, reaches a saturation value at approx. 8 *eV*. The photon-energy dependence of ε_{eff} shows us a rapid rise that extends up to 5 *eV*. Then the value of ε_{eff} rises more smoothly and slowly and tends to saturate at the energy 8 *eV*. This means that the greatest contribution to ε_{eff} arises from interband transitions between 1 *eV* and 5 *eV*.

As stated above, the N_{eff} determined from the sum rule (Eq. 9) is the effective number of valance electrons per unit cell at the energy $\hbar\omega_0$ (under the condition that all of the interband transitions possible at this frequency ω_0 were made). In the case of Bi_2S_3 and Bi_2Se_3 the value of N_{eff} increases with increasing photon energy and has a tendency to saturate near 8 *eV* and 20 *eV* (see Fig. 7). Therefore, each of our plots of N_{eff} versus the photon energy for Bi_2S_3 and Bi_2Se_3 can be arbitrarily divided into two parts. The first is characterized by a rapid growth of N_{eff} up to ~6 *eV* and extended to 9 *eV*. The second part shows a smoother and slower growth of N_{eff} and tends to saturate at energies above 30 *eV*. It is therefore, rather difficult to choose independent criteria for the estimate of the valance electrons per unit cell. Recognizing that the two valance subbands are separated from each other and are also separated from the low-lying states of the valance band, we can assume a tendency to saturation at energies such that the transition from the corresponding subbands are exhausted. In other words, since N_{eff} is determined only by the behavior of ε_2 and is the total oscillator strengths, the sections of the N_{eff} curves with the maximum slope, which correspond to the maxima $dN_{eff}/d\hbar\omega$, can be used to discern the appearance of a new absorption mechanism with increasing energy (E=5.2 *eV*, 8.6 *eV* for Bi_2S_3 and E=5.0 *eV*, 9 *eV* for Bi_2Se_3). The values and behavior of N_{eff} and ε_{eff} for both directions are very close to each other.

By using our results from "Elastic properties" and "Optical properties" we also calculated elasto-optic tensors for Bi_2S_3

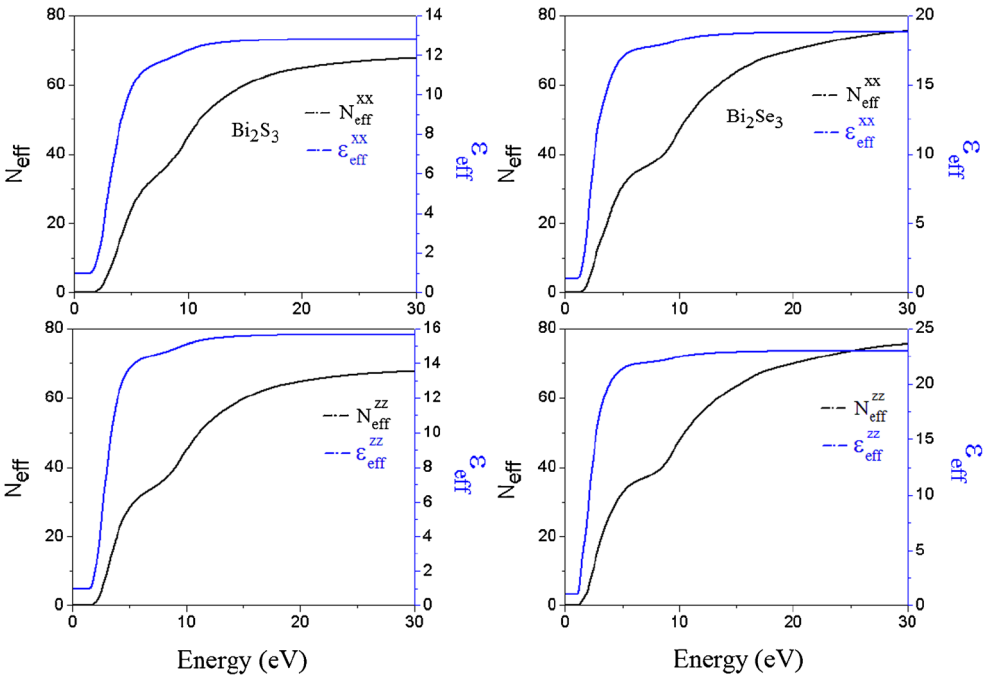

Fig. 7 Energy spectra of N_{eff} and ε_{eff} along the x- and z- axes

and Bi_2Se_3. It is well known that in order to describe the elasto-optic effect we must use the usual definition and relate optical impermeability-κ (inverse dielectric constant) to strain tensor C_{ij} via a fourth-rank elasto-optic p tensor in order to describe the elasto-optic effect. The impermeability change is then given in terms of the elasto-optic p coefficients and electro-optic f coefficients by the expression

$$\Delta\left(\frac{1}{n^2}\right)_{ij} = \sum_{k,l} p_{ijkl}{}^{\mathrm{P}} C_{kl} + \sum_{k} f_{ijk}{}^{C}\mathrm{P}_k, \tag{12}$$

where the superscripts C and P denote that these coefficients are measured at constant strain and constant polarization, respectively [73].

The elasto optic coefficients form a fourth rank tensor p defined by the equation:

$$p_{ijkl} = \partial\kappa_{ij}/\partial S_{kl} \tag{13}$$

where S is the strain tensor. In their common principal coordinate system, the diagonal elements of the permittivity and impermittivity tensors are direct reciprocals. Hence,

$$(\partial\kappa/\partial y)_{ij} = \left(\partial/\partial_y\right)\left(\varepsilon^{-1}\right)_{ij} = -\left(1/\varepsilon_{ii}\varepsilon_{jj}\right)\left(\partial\varepsilon_{ji}/\partial_y\right), \tag{14}$$

where y is any independent variable. Although the off-diagonal elements are zero, by definition, in the principal coordinate system, their derivatives with respect to an independent variable need not be zero. The symmetry of orthorhombic allows only 12 independent elasto-optic coefficients [79]. In the reduced index notation, the elasto-optic matrix for orthorhombic Bi_2S_3 and Bi_2Se_3 compounds are:

$$\mathrm{P} = \begin{bmatrix} p_{11} & p_{12} & p_{13} & 0 & 0 & 0 \\ p_{21} & p_{22} & p_{23} & 0 & 0 & 0 \\ p_{31} & p_{32} & p_{33} & 0 & 0 & 0 \\ 0 & 0 & 0 & p_{44} & 0 & 0 \\ 0 & 0 & 0 & 0 & p_{55} & 0 \\ 0 & 0 & 0 & 0 & 0 & p_{66} \end{bmatrix} \tag{15}$$

with the nonzero elements. Thus, for components involving diagonal strain elements, only diagonal permittivity elements need to be considered. A typical elasto-optic coefficient is

$$p_{ijkl} = \partial\kappa_{ij}/\partial S_{kl} = -\left(1/\varepsilon_{ii}\varepsilon_{jj}\right)\left(\partial\varepsilon_{ij}/\partial S_{kl}\right) \tag{16}$$

that we calculated by using results from "Elastic properties" and "Optical properties" and Eqs. 15 and 16. The results are shown below.

$$\mathrm{P}_{Bi_2S_3} = \begin{bmatrix} 0.43 & 0.96 & -0.73 & 0 & 0 & 0 \\ 0.96 & 0.32 & 0.90 & 0 & 0 & 0 \\ -0.73 & 0.90 & 0.36 & 0 & 0 & 0 \\ 0 & 0 & 0 & 0.57 & 0 & 0 \\ 0 & 0 & 0 & 0 & 0.51 & 0 \\ 0 & 0 & 0 & 0 & 0 & 0.92 \end{bmatrix} \tag{17}$$

$$\mathrm{P}_{Bi_2Se_3} = \begin{bmatrix} 0.23 & 0.47 & -0.39 & 0 & 0 & 0 \\ 0.47 & 0.28 & 0.27 & 0 & 0 & 0 \\ -0.39 & 0.27 & 0.29 & 0 & 0 & 0 \\ 0 & 0 & 0 & 0.23 & 0 & 0 \\ 0 & 0 & 0 & 0 & 0.18 & 0 \\ 0 & 0 & 0 & 0 & 0 & 0.39 \end{bmatrix} \tag{18}$$

Conclusions

We studied the structural, electronic, mechanical, and optical properties of the Bi_2S_3 and Bi_2Se_3 compounds using first principle DFT methods. The calculated lattice parameters and internal coordinates are in agreement with the experimental results. The elastic constants were obtained using the "volume-conserving" technique and strain–stress relationship. The results indicate that these compounds are mechanically stable. Due to the higher value of Young's modulus, the Bi_2S_3 compound is relatively stiffer than Bi_2Se_3. In addition, the calculated bulk modulus, shear modulus, Debye temperature, and wave velocity for Bi_2S_3 are higher than Bi_2Se_3. Moreover, both compounds for SIESTA calculations are classified as being brittle, and for VASP calculations are classified as being ductile. The ionic contribution to inter atomic bonding for these compounds is dominant. We have revealed that the band structures of these compounds are a semiconductor in nature. We have examined the photon-energy dependent dielectric functions, some optical properties such as the energy-loss function, the effective number of valance electrons, the effective optical dielectric constant along the x- and z- axes and elasto-optical coefficients under pressure.

References

1. Ryu S, Schnyder AP, Furusaki A, Ludwing AWW (2010) New J Phys 12:065010.1–065010.60
2. Zhang W, Yu R, Zhang HJ, Dai X, Fang Z (2010) New J Phys 12: 065013.1–065013.14
3. Zhang H, Liu CH, Qi XL, Dai X, Fang Z, Zhang SC (2009) Nat Phys 5:438–442

4. Liang, Kane CL, Mele EJ (2007) Phys Rev Lett 98:106803.1–106803.4
5. Suarez R, Nair PK, Kamat PV (1998) Langmuir 14:3236–3241
6. Chen B, Uher C (1997) Chem Mater 9:1655–1658
7. Rabin O, Perez JM, Grimm J, Wojtkiewicz G, Weissleder R (2006) Nat Mater 5:118–122
8. Zhang B, Ye X, Hou W, Zhao Y, Xie YJ (2006) J Phys Chem B 110: 8978–8985
9. Li L, Cao R, Wang Z, Li J, Qi L (2009) J Phys Chem C 113:18075–18081
10. Black J, Conwell EM, Seigle L, Spenser W (1957) J Phys Chem Solids 2:240–251
11. Riley DJ, Waggett JP, Wijayantha KGU (2003) J Mat Chem 14:704–708
12. Cademartiri L, Malakooti R, Brien PGO, Migliori A, Petrov S (2008) Angew Chem Int Ed 20:3811–3817
13. Begum A, Hussain A, Rahman A (2011) Mater Sci Appl 2:163–168
14. Gordyakova GN, Sinani SS (1958) Sh Tekh Fiz 28:977–988
15. Shah MP, Holmberg SH, Kostylev SA (1973) Phys Rev Lett 31:542–545
16. Keneman SA (1971) Appl Phys Lett 19:205–207
17. Goto N, Ashikawa MJ (1970) Non-Cryst Solids 4:378–379
18. Tokwda W, Katoh T, Yasumori A (1974) J Appl Phys 45:5098–5099
19. Frerich RJ (1953) Opt Soc Am 43(1953):1153–1157
20. Kolomiets BT, Pavlov BV (1960) Soc Phys Solid State 2:592–597
21. Ghosh B, Kothiyal GP (1983) Prog Cryst Growth Charact 6:393–413
22. Han Q, Chen J, Yang X, Lu L, Wan X (2007) J Phys Chem C 111: 14072–14077
23. Caracas R, Gonze X (2005) Phys Chem Miner 32:295–300
24. Sharma Y, Srivastava P, Dashora A, Vadkhiya L, Bhayani MK, Jain R, Jani AR, Ahuja BL (2012) Solid State Sci 14:241–249
25. Sharma Y, Srivastava P (2010) AIP Conf Proc 1249:183
26. Olsen LA, López-Solano J, García A, Balić-Žunic T, Makovicky E (2010) J Solid State Chem 183:2133–2143
27. Filip MR, Patrick CE, Giustino F (2013) Phys Rev B 87:205125.1–205125.11
28. Zhao Y, Chua KTE, Gan CK, Zhang J, Peng B, Peng Z, Xion Q (2011) Phys Rev B 84:205330.1–205330.8
29. Hasan MZ, Kane CL (2010) Rev Mod Phys 82:3045–3067
30. Molotkov SN, Potapov TA (2013) JETP Lett 98:298–303
31. Sankey OF, Niklewski DJ (1989) Phys Rev B 40:3979–3995
32. Ordejón P, Artacho E, Soler JM (1996) Phys Rev B 53:R10441–R10444
33. Soler JM, Artacho E, Gale JD, García A, Junquera J, Ordejón P, Sánchez-Portal D (2002) J Phys Condens Matt 14:2745–2779
34. Kohn JW, Sham LJ (1965) Phys Rev 140(1965):A1133–A1138
35. Ceperley DM, Adler MJ (1980) Phys Rev Lett 45:566–569
36. Perdew P, Zunger A (1981) Phys Rev B 23:5048–5079
37. Troullier N, Martin JL (1991) Phys Rev B 43:1993–2006
38. Kresse G, Hafner J (1994) Phys Rev B 47:558–561
39. Kresse G, Furthmuller J (1996) Comp Mater Sci 6:15–50
40. Kresse G, Joubert D (1999) Phys Rev B 59:1758–1775
41. Kresse G, Furthmuller J (1996) Phys Rev B 54:11169–11186
42. Blochl PE (1994) Phys Rev B 50:17953–17979
43. Monkhorst HJ, Pack JD (1976) Phys Rev B 13:5188–5192
44. Kanishcheva AS, Mikhailav YN, Trippel AF (1981) Izv Akad Nauk SSSR Neorg Mater 17:1972–1975
45. Atabaeva EY, Mashkov SA, Popov SV (1973) Kristallografiya 18: 173–174
46. Murnaghan FD (1944) Proc Natl Acad Sci U S A 50:244–247
47. Deligoz E, Ozisik H, Colakoglu K, Surucu G, Ciftci YO (2011) J Alloy Comp 509:1711–1715
48. Ateser E, Ozisik H, Colakoglu K, Deligoz E (2011) Comp Mater Sci 50:3208–3212
49. Wallace DC (1972) Thermodynamics of Crystals, Chap. 1, where finite Lagrangian strains ηij are discussed. In the case of infinitesimal strains these reduce to our εij of classical elasticity theory. Wiley, New York
50. Le Page Y, Saxe P (2001) Phys Rev B 63:174103.1–174103.8
51. Beckstein O, Klepeis JE, Hart GLW, Pankratov O (2001) Phys Rev B 63:134112.1–134112.12
52. Voight W (1928) Lehrbook der kristallphysik. Teubner, Leipzig, p 962
53. Reuss AZ (1929) Angew Math Mech 9:49–58
54. Hill R (1952) Proc Phys Soc London Sect A 65:349–354
55. Panda KB, Chandran KSR (2006) Acta Mater 54(2006):1641–1657
56. Ravindran P, Fast L, Korzhavyi PA, Johansson B, Wills J, Eriksson O (1998) J Appl Phys 84:4891–4904
57. Koc H, Mamedov AM, Deligoz E, Ozisik H (2012) Solid State Sci 14:1211–1220
58. Koc H, Deligöz E, Mamedov AM (2011) Phys Mag 91:3093–3107
59. Shein IR, Ivanovskii AL (2008) J Phys Considens Matter 20: 415218.1–415218.9
60. Pogh SF (1954) Philos Mag 45:833–838
61. Bannikov VV, Shein IR, Ivanovskii AL (2007) Phys Stat Sol (RRL) 3:89–91
62. Fu H, Li D, Eng F, Gao T, Cheng X (2008) Comp Mater Sci 44:774–778
63. Tvergaard V, Hutchinson JW (1988) J Am Chem Soc 71:157–166
64. Chung DH, Buessem WR (1968) In: Vahldiek FW, Mersol SA (eds) Anisotropy in single crystal refractory compounds. Plenum, New York, p 217
65. Johnston I, Keeler G, Rollins R, Spicklemire S (1996) Solids state physics simulations, the consortium for upperlevel physics software. Wiley, New York
66. Anderson OL (1963) J Phys Chem Solids 24:909–917
67. Schreiber E, Anderson OL, Soga N (1973) Elastic constants and their measurements. McGraw-Hill, New York
68. Chen X-Q, Niu H, Li D, Li Y (2011) Intermetallics 19:1275–1281
69. Mahmoud S, Eid AH, Omar H (1997) Fizika A 6:111–120
70. Al-Douri AAJ, Madik MP (2000) Renew Energy 21:411–416
71. Qui XF, Austin LN, Muscarella PA, Dyck JS, Burda C (2006) Angew Chem Int Ed 45:5656–5659
72. Yesugade NS, Lokhande CD, Bhosak CH (1955) Thin Solid Films 263:145–149
73. Wemple SH, Di Domenico M (1970) Phys Rev B 1:193–202
74. Levine ZH, Allan DC (1989) Phys Rev Lett 63:1719–1722
75. Philipp HR, Ehrenreich H (1963) Phys Rev 129:1550–1560
76. Koc H, Mamedov AM, Ekmel O (2013) Ferroelectrics 448:29–41
77. Kovalev OV (1965) Representations of the crystallographic space groups. Irreducible representations induced representations and corepresentations. Gordon and Breach, Amsterdam
78. Marton L (1956) Rev Mod Phys 28:172–183
79. Kohn ES (1969) J Appl Phys 40:2608–2613